https://doi.org/10.5194/egusphere-2023-127
Preprint. Discussion started: 10 March 2023

Fine particle chemistry under a special dust transport event: impacts from unusually enhanced ozone and air mass backflows over the ocean

Da Lu[1], Hao Li[1], Guochen Wang[1], Xiaofei Qin[1], Na Zhao[1], Juntao Huo[2], Fan Yang[3], Yanfen Lin[2], Jia Chen[2], Qingyan Fu[2], Yusen Duan[2], Xinyi Dong[4], Congrui Deng[1], Sabur F. Abdullaev[5], Kan Huang[1,6*]

[1]Center for Atmospheric Chemistry Study, Shanghai Key Laboratory of Atmospheric Particle Pollution and Prevention (LAP[3]), National Observations and Research Station for Wetland Ecosystems of the Yangtze Estuary, Department of Environmental Science and Engineering, Fudan University, Shanghai, 200433, China

[2]State Ecologic Environmental Scientific Observation and Research Station for Dianshan Lake, Shanghai Environmental Monitoring Center, Shanghai, 200030, China

[3]Pudong New District Environmental Monitoring Station, Shanghai 200122, China

[4]School of Atmospheric Sciences, Nanjing University, Nanjing 210023, China

[5]Physical Technical Institute of the Academy of Sciences of Tajikistan, Dushanbe, Tajikistan

[6]Institute of Eco-Chongming (IEC), Shanghai, 202162, China

Corresponding author: huangkan@fudan.edu.cn

Abstract

A five-days long-lasting dust event was observed with a synergy of field measurements techniques in Shanghai in the autumn of 2019. Different from most dust

https://doi.org/10.5194/egusphere-2023-127
Preprint. Discussion started: 10 March 2023

events, this dust was an unusual one characterized of low wind speed, high relative humidity, high concentrations of gaseous precursors, and contrasting wind vectors between low and high altitudes. Three dust stages were identified and the first stage was a normal dust invasion with high particulate concentrations and short duration. In contrast, unusual enhancement of ozone was observed in the second stage, due to compound causes of weak synoptic system, transport from the ocean, and subsidence of high-altitude O_3 down drafted by dust. As a result, sulfate and nitrate moderately correlated with O_3 while had almost no correlation with aerosol liquid water content, indicating the dominant role of gas phase oxidations. During the third stage of dust, a special phenomenon of dust backflow was observed that the dust plume drifted from the Shandong Peninsula and travelled slowly over the Yellow Sea and the East China Sea, finally returning to Shanghai. The dust backflow was evidenced by the enrichment of marine vessel emissions (V and Ni) and increased solubility of calcium. Under the humid oceanic breezes, the formation of nitrate was dominated by aqueous processing, while the strong correlation between SO_4^{2-} and Na^+ suggested that a considerable part of sulfate was aged and directly transported. Based on the thermodynamic modeling, sea salts probably involved more in the secondary aerosol formation than the dust heterogeneous reactions. By developing an upstream-receptor relationship method, the amounts of transported and secondarily formed aerosol species were separated. This study highlights that the transport pathway of dust and environmental conditions could significantly modify the aerosol properties, especially at the complex land-sea interface.

1. Introduction

As an important source of natural aerosols, dust accounted for about half of the

https://doi.org/10.5194/egusphere-2023-127
Preprint. Discussion started: 10 March 2023

tropospheric aerosols (Zheng et al., 2016). Dust aerosols played important roles in environmental and climatic changes by affecting the radiation balance (Feng et al., 2020; Nagashima et al., 2016; Goodman et al., 2019). Furthermore, dust aerosols had important influences on tropospheric chemistry by participating in heterogeneous and photolysis reactions in the atmosphere (Wang et al., 2014; Xu et al., 2018). For instance, dust could mix with gaseous pollutants, toxic metals, and soot during transport, thus affecting air quality immediately and causing potential public health hazards (Liu et al., 2021; Wang et al., 2021). Moreover, Barkley et al. (2021) found that iron-containing aerosols transported from Africa to the equatorial North Atlantic Ocean provided plentiful nutrients to algae in the ocean and accumulated inside algae.

Many studies focused on the emissions and transport of Asian dust, which accounted for ~20% of the global dust budget (Ginoux et al., 2004). Asian dust mostly originated from the deserts in western China, the Gobi, and the Loess Plateau (Nagashima et al., 2016). Dust particles can be lifted to an altitude of several kilometers due to strong winds and low soil moistures. During this process, most of the coarse dust particles would settle near the dust source areas, while relatively fine particles could be transported to further downstream regions such as eastern and southern China, and even across the Pacific Ocean to the western America coast (Fu et al., 2010; Vicars and Sickman, 2011).

The irregular shapes of dust particles provided efficient medium for heterogeneous reactions with NO_2, O_3, SO_2, and NH_3, thus changing the particle size spectrum, hygroscopicity, and radiative properties (Hsu et al., 2014; Tian et al., 2021; Wang et al., 2018a). Wang et al. (2018a) observed that the concentrations of nitrate and sulfate were significantly elevated due to the moderate/high levels of relative humidity

https://doi.org/10.5194/egusphere-2023-127
Preprint. Discussion started: 10 March 2023

and gaseous precursors during a dust period in March, 2010 at Shanghai, implying that dust can efficiently promoted the formation of sulfate and nitrate. The formation of nitrate included two major pathways. During daytime, the OH radicals produced by the photolysis of O_3 and HONO oxidized NO_2 to produce HNO_3 (Hertel et al., 2012), which subsequently neutralized the alkaline substances to form nitrate in the particles. During nighttime with low temperature and high humidity, NO_2 can be oxidized by O_3 to form NO_3 radical (Mentel et al., 1996), which then reacted with NO_2 to form N_2O_5 radical (Dall'osto et al., 2009; Petetin et al., 2016). Previous studies have revealed that HNO_3 formed through the reactions of NO_2 with hydroxyl radical or N_2O_5 hydrolysis would preferentially react with mineral dust particles and produce nitrate, which was the main source of nitrate during the dust period (Tang et al., 2016; Wu et al., 2020). Wang et al. (2018b) found that the heterogeneous reactions on the dust surface were the main sources of nitrate, and the dust surface nitrate observed in Japan mainly formed over the Yellow Sea and the East China Sea during the long-range transport.

However, there were some controversies on the mixing of dust and anthropogenic aerosols. Zhang et al. (2005) found that anthropogenic aerosols separated with dust during a dust event in Qingdao, China. Coincidentally, there existed a time-lag between dust and anthropogenic aerosols in Japan and South Korea downstream of the dust transport. Single particle analysis confirmed that sulfate in fine particles appeared 12 hours before the dust arrival in Japan. Wang et al. (2013) also observed a 10 - 12 hours lag between dust and anthropogenic aerosols in a dust day in Shanghai (Wang et al., 2013). Furthermore, Huang et al. (2019) observed that there were vertical differences of the long-transported aerosols during a pollution event in Taiwan. Dust from the Gobi Desert in Inner Mongolia and China existed at the altitudes of 0.8km and 1.90km,

https://doi.org/10.5194/egusphere-2023-127
Preprint. Discussion started: 10 March 2023

respectively, while biomass burning aerosols from South Asia existed at higher altitudes of 3.5km.

In the coastal regions, the regional pollution was always a mix of inland anthropogenic emissions and ocean-sourced releases. Due to the active human activities and special weather conditions such as monsoon and sea-land breezes, the atmospheric compound pollution was usually more complex in the coastal areas (Wang et al.; Hilario et al., 2020; Patel and Rastogi, 2020; Perez et al., 2016; Wang et al., 2017). The eastern coast of China is bordering the East China Sea and the Yellow Sea and is strongly influenced by the Asian monsoon and high emissions from inland industries. The meteorological conditions and pollution conditions in this region were among the most complex in the world (Hilario et al., 2020). Due to the complex meteorological conditions, the relative humidity and temperature of the marine boundary layer showed significant seasonal and diurnal changes, further affecting the photochemical processes and the heterogeneous reactions on the aerosol surface (Zhao et al., 2021). Under the influence of sea and land breezes, land breezes at night blew the land pollutants to the sea. In the next day, land breezes would evolve as sea breezes and return the pollutants over the sea to the land, resulting in the increase of air pollutants over the land (Zhao et al., 2021). High relative humidity caused by the sea breeze favored the participation of gaseous precursors in heterogeneous reactions, hygroscopic growth of particles, and secondary aerosol formation. Sun et al. (2020) found that nitrate was the main species of aerosol in Shanghai during pollution events from 2017-2018, while most of these events in winter were caused by the long-transport of air pollutants from the North China Plain. Sea salt, as an important component of aerosol in coastal areas, has been found in various studies that complex multiphase reactions can occur on the surface of

https://doi.org/10.5194/egusphere-2023-127
Preprint. Discussion started: 10 March 2023

sea salts (Fu et al., 2010; Patel and Rastogi, 2020; Wang et al., 2022a). Wang et al. (2022a) found that the addition of Na^+ in the ISORROPIA model improved the simulation performance of aerosol and gaseous species at a coastal site in the South China Sea, indicating that sea salts participated in the heterogeneous reactions with other aerosol species. Liang et al. (2018) found that the rise of O_3 in Shanghai could be affected by both local secondary formation and marine transport based on observation and simulation. Meanwhile, Wang et al. (2022b) found that during the ozone pollution in Shanghai in 2018, the presence of O_3 at high altitudes at night was transported vertically downward during the daytime and high O_3 over the ocean was transported horizontally to the land, thus jointly causing regional O_3 pollution in Shanghai.

Previous studies have shown that about 70% of Asian dust would pass through the eastern coast of China and then moved out over Korean Peninsula and the Sea of Japan, finally ending at the Pacific Ocean. The eastern coast of China is considered as the essential route of the Asian dust transport to the Pacific Ocean (Arimoto et al., 1997; Huang et al., 2010). In this study, an atypical dust event was observed in Shanghai, a coastal mega-city in Eastern China. The unusualness of the meteorological conditions and air pollutants during the dust was explicitly described. Three stages of the dust were sorted and aerosol chemical compositions were compared. By focusing on the second and third stages, the different formation mechanisms of nitrate and sulfate were investigated. The amounts of major aerosol species from transport and secondary formation were estimated based on a simple method of relating the upstream and receptor simultaneous measurements.

2. Methodology

https://doi.org/10.5194/egusphere-2023-127
Preprint. Discussion started: 10 March 2023

2.1. Observational sites

Measurements of various atmospheric parameters were conducted at Shanghai Pudong Environmental Monitoring Station (31°13′ N, 121°32′E). All the instruments were set up on the top floor of the building, about 25m above the ground. As shown in Figure 1, the sampling site was located at the eastern tip of Shanghai, close to the coastal line. The mean temperature and relative humidity were 17.3℃ and 72% in Shanghai during November, respectively. In autumn and winter, air pollutants from upstream urban regions could be frequently transported to Shanghai via the high-pressure system. Furthermore, air pollutants in Shanghai tended to linger at the sea/land boundary regions due to the sea-land breeze (Shen et al., 2019).

In addition to the measurements in Shanghai, data from environmental monitoring stations in Qingdao and Lianyungang are also used in this study.

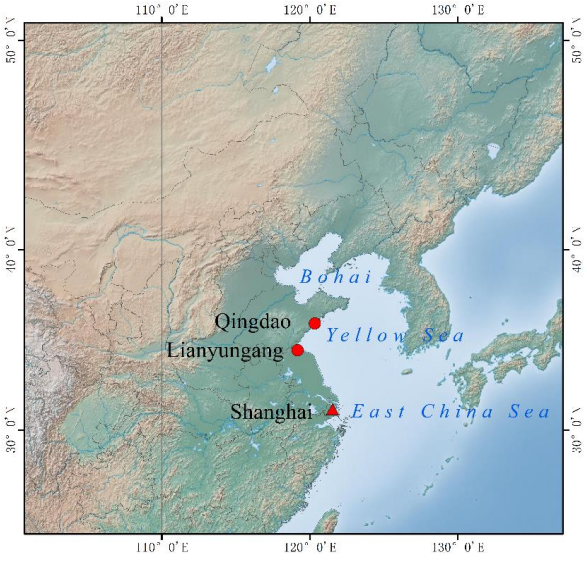

Figure 1. The observational sites in this study, including Shanghai, Qingdao, and

https://doi.org/10.5194/egusphere-2023-127
Preprint. Discussion started: 10 March 2023

Lianyungang.

2.2. Instrumentation

A set of online instruments was set up at the Pudong observational site. Inorganic ions (NO_3^-, SO_4^{2-}, Cl^-, Na^+, NH_4^+, K^+, Mg^{2+}, Ca^{2+}) in $PM_{2.5}$ and soluble gases (NH_3, HNO_3, HCl, HONO) were measured by an online ion chromatography (IC, MARGA-1S, Metrohm). It operated at a flow rate of 16.7 L/min with a time resolution of one hour. Briefly, air was drawn into a $PM_{2.5}$ cyclone inlet and passed through a wet rotating denuder (gases) and a steam jet aerosol collector (aerosols). Subsequently, the aqueous samples were analyzed with ion chromatography. More details can be found in (Xu et al., 2020). Hourly trace metals (Si, Ca, Cu, Fe, K, Co, Mn, Cr, Zn, Pb, As, Cd, V, Ni) in $PM_{2.5}$ were measured by using the Xact 625 multi-metals monitor (Cooper Environmental, Beaverton, OR, USA). Particles were collected onto a Teflon filter tape at a flow rate of 16.7 L/min, and then transported into the spectrometer where the particles were analyzed with an X-ray fluorescence. Organic carbon and elemental carbon were measured by an in situ Semi-Continuous Organic Carbon and Elemental Carbon aerosol analyzer (RT-4, Sunset Laboratory, Beaverton, Oregon, USA).

The concentrations of particles and gaseous pollutants were measured by a set of Thermo Fisher Scientific instruments, including $PM_{2.5}$ (Thermo 5030i), PM_{10} (Thermo 5030i), SO_2 (Thermo Fisher 43i), NO_x (Thermo Fisher 42i), O_3 (Thermo Fisher 49i), and CO (Thermo Fisher 48i-TLE). Meteorological parameters (ambient temperature, relative humidity, wind speed, and wind direction) were obtained by a Vaisala Weather transmitter (WXT520). Other supplementary parameters such as the height of planetary

https://doi.org/10.5194/egusphere-2023-127
Preprint. Discussion started: 10 March 2023

boundary layer (PBL), vertical profiles of ozone and aerosol extinction were obtained by a ceilometer (CL31, Vaisala), ozone lidar (LIDAR-G-2000, WUXIZHONGKE), and aerosol lidar (AGJ, AIOFM), respectively.

2.3. Thermodynamic simulation of aerosol pH and aerosol liquid water content

The ISORROPIA II model is subject to the principle of minimizing the Gibbs energy of the multi-phase aerosol system, leading to a computationally intensive optimization problem (Song et al., 2018). ISORROPIA II calculates the aerosol pH, ALWC (aerosol liquid water content) and compositions of ammonia-sulfate-nitrate-chloride-sodium-calcium-potassium-magnesium in the thermodynamic equilibrium with gas-phase precursors. The performances and advantages of ISORROPIA over the usage of other thermodynamic equilibrium codes has been assessed in numerous studies (Nenes et al., 1998; West et al., 1999; Ansari and Pandis, 1999; Yu et al., 2005). The ISORROPIA running in the forward mode at the metastable state was applied in this study.

2.4. Hybrid Single-Particle Lagrangian Integrated Trajectory Model

The HYSPLIT (Hybrid Single-Particle Lagrangian Integrated Trajectory) was used to compute the backward trajectories of the air parcels during the dust events. In this study, the HYSPLIT model was driven by meteorological data outputs from the Global Data Assimilation System (GDAS) (Su et al., 2015), which is available at ftp://arlftp.arlhq.noaa.gov/pub/archives/gdas1. Air mass trajectories were launched at different heights from the ground and a total duration of 48 hours simulation was conducted.

https://doi.org/10.5194/egusphere-2023-127
Preprint. Discussion started: 10 March 2023

3. Results and Discussion

3.1. Characteristics of an unusual dust event

Figure 2 shows the time series of PM_{10}, $PM_{2.5}$, and meteorological parameters as well as the vertical profiles of aerosol extinction coefficient and depolarization ratio observed at the Shanghai sampling site from October 25 to November 6, 2019. During October 25 to 28, the mean wind speed was relatively low of 0.9±0.72m/s with the peak value of 3.1m/s and winds prevailed from the northwest. The mean concentration of $PM_{2.5}$ and PM_{10} was 34.7 and 44.2 μg/m^3, respectively. Starting at 4:00 LST on October 29, the concentration of PM_{10} increased sharply and lasted till November 2 (Figure 2d). Based on the aerosol lidar observation, both aerosol extinction coefficient and depolarization ratio extended from the ground to around 2km during the same period. Specifically, the depolarization ratio was obviously enhanced (>0.1), indicating that Shanghai encountered a long-lasting dust event. During the whole dust period, the mean concentrations of $PM_{2.5}$ and PM_{10} reached 53.3 ± 20.5μg/m^3 and 172.4 ± 70.2μg/m^3, respectively, yielding a low $PM_{2.5}/PM_{10}$ ratio of 0.34 ± 0.15. As a comparison, $PM_{2.5}$ and PM_{10} during the non-dust period was 38.9μg/m^3 and 49.8μg/m^3, respectively, with a relatively high $PM_{2.5}/PM_{10}$ ratio of 0.62 ± 0.20.

https://doi.org/10.5194/egusphere-2023-127
Preprint. Discussion started: 10 March 2023

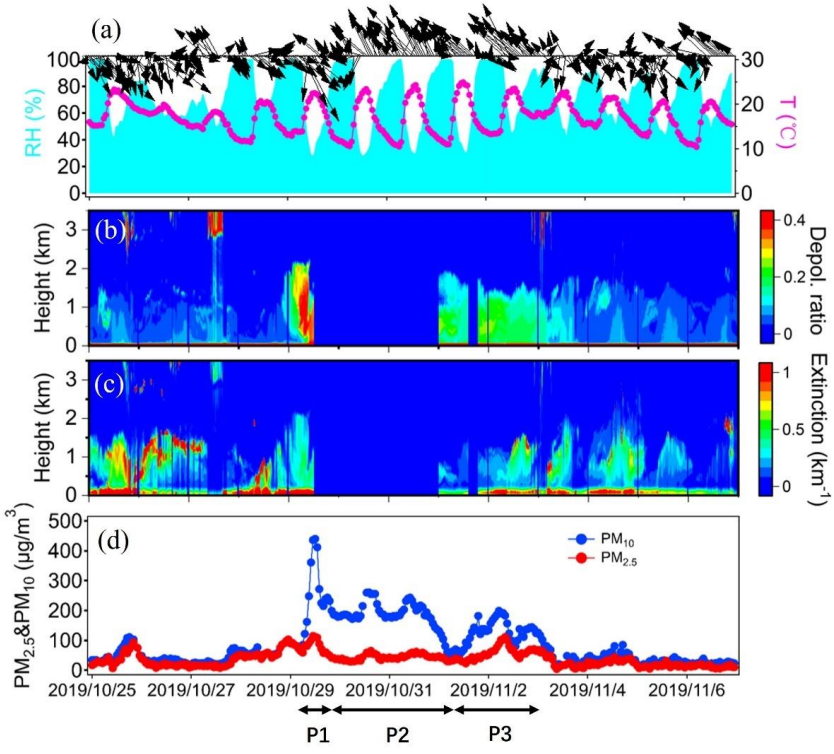

Figure 2. Time series of (a) relative humidity, temperature, wind vectors, (b) aerosol depolarization ratio, (c) aerosol extinction coefficient, (d) mass concentrations of $PM_{2.5}$ and PM_{10} during the study period. Three dust stages, i.e., P1, P2, and P3 are also marked. The missing aerosol lidar data were due to instrument malfunction.

The occurrences of dust were usually accompanied by low relative humidity and strong winds due to the passage of cold fronts (Fu et al., 2010; Huang et al., 2010; Wang et al., 2013; Wang et al., 2018b). In this study, relative humidity was exceptionally high with the mean value of 71±26%. It showed strong diurnal variation with minimum in the daytime and even close to 100% in the nighttime (Figure 2a). Also, wind speed was low of 0.54±0.59m/s with a maximum of 2.6m/s. Due to this stagnant synoptic condition, the mean concentrations of main gaseous pollutants such as O_3, SO_2, and

https://doi.org/10.5194/egusphere-2023-127
Preprint. Discussion started: 10 March 2023

NO_2 reached 86.0±47.8μg/m^3, 11.8±3.4μg/m^3, and 63.3±27.9μg/m^3, respectively, even higher than those during the non-dust period.

We further divided the dust event into three stages based on the temporal characteristics of PM_{10} and the air masses transport patterns. As shown in Figure 2d, PM_{10} quickly climbed from 4:00 on October 29 and reached a maximum of 436μg/m^3 after 8 hours. The air masses mainly originated from the semi-arid regions of northwest China (Figure 3d), and this was consistent with both near surface wind observation (Figure 2a) and wind lidar observation (Figure 3a). The wind profiles showed dominant northwest winds from the ground to the altitudes of around 2km before the noon of October 29, indicating the presence of a strong synoptic system. Afterwards, PM_{10} quickly decreased to 199 μg/m^3 at 20:00, October 29 within 8 hours. This was mainly due to the shift of wind directions. As shown in Figure 3a, although the winds at altitudes of higher than 700m kept blowing from the northwest, the near surface winds had turned from the southeast. As Shanghai is a coastal city and adjacent to the East China Sea, the relatively clean southeasterlies diluted the local air pollutants and thus explained the quick decrease of PM_{10} concentrations. This short dust episode from 4:00 - 13:00, October 29 was defined as Stage P1.

However, the prevailing southeast winds didn't fully terminate the dust event. Even under the persistent southeasterlies, hourly PM_{10} concentrations stayed above 150 μg/m^3 until November 1 and then decreased to 65 μg/m^3 at 03:00, November 1 (Figure 2d). Compared to P1, wind speed during this stage was as low as 0.4 ± 0.5m/s while RH was moderately high of 70 ± 26%. Although the daytime RH stayed low between 30% and 50%, it frequently reached over 90% at nighttime. Figure 3e shows that although the air masses originated from the Gobi Desert, they also passed over

https://doi.org/10.5194/egusphere-2023-127
Preprint. Discussion started: 10 March 2023

considerable coastal regions. The wind profiles also showed that although northwest winds prevailed at altitudes higher than 500m, the east and northeast winds were dominant below 500m (Figure 3b). This explained the relatively high relative humidity during this period due to the mixing between dust plumes and coastal sea breezes. This dust episode from 14:00, October 29 to 3:00, November 1 was defined as Stage P2.

After P2, PM_{10} and $PM_{2.5}$ rose again and peaked at 5:00 and 9:00, November 2 with the hourly concentration of 199 and 117μg/m^3, respectively. Different from P1 and P2, the air masses originated from the Shandong Peninsula and the northern region of Jiangsu province, and then migrated over the Yellow Sea and the East China Sea (Figure 3f). Usually, the dust plumes would transport further eastwards and impact the western Pacific region and even faraway oceanic regions (Wang et al., 2018b; Nagashima et al., 2016). However, the air masses evidently deflected and pushed the dust back to the mainland. The wind profiles on November 2 also showed winds at the detected range of altitudes all came from the eastern and southeastern oceanic regions (Figure 3c). This probably indicated the mixing between dust plumes and humid oceanic air masses was quite sufficient, which was also reflected by the highest average RH of 76 ± 24% among the three stages of the dust event. In addition, the concentrations of O_3 and NO_2 at this stage were higher than those of P1 and P2, which could be conducive to the formation of secondary aerosol components and will be discussed later. This rarely observed dust backflow transport episode from 4:00, November 1 to 23:00, November 2 was defined as Stage P3.

https://doi.org/10.5194/egusphere-2023-127
Preprint. Discussion started: 10 March 2023

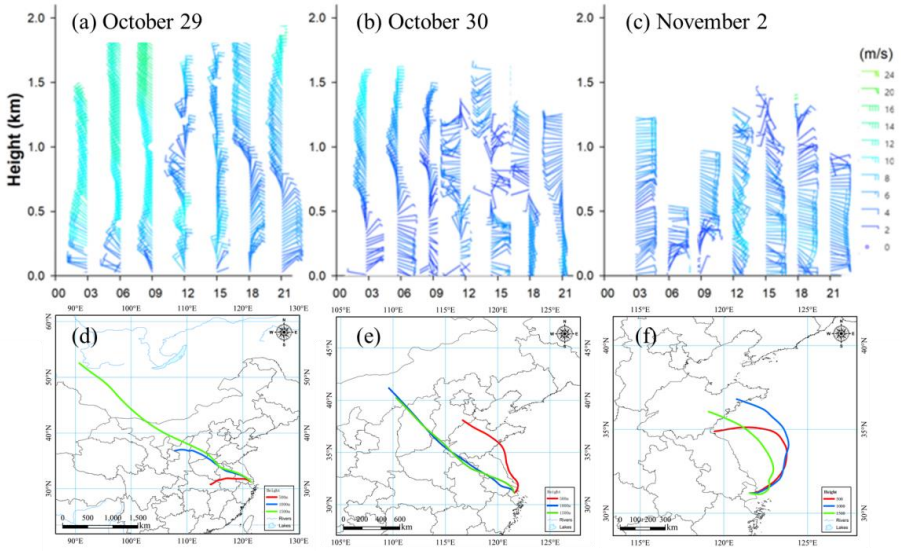

Figure 3. Wind profiles observed by a wind profiler radar on (a) October 29, (b) October 30, and (c) November 2. 48-hour backward trajectories simulated at the sampling site starting from (d) 4:00 AM, October 29, (e) 9:00 AM, October 30, and (f) 13:00 PM, November 2. The red, blue, and green trajectories represented starting altitudes of 100, 500, and 1500m, respectively.

3.2. Comparisons of aerosol chemical compositions among the three dust stages

Figure 4a shows the time-series of hourly aerosol chemical components, including SNA (NO_3^-, SO_4^{2-}, and NH_4^+), OM (organic matters = 2*OC), EC, and mineral aerosols ([Minerals]= (2.2*Al+2.49*Si+1.63*Ca+2.42*Fe+1.94*Ti), (Malm et al., 1994)) in $PM_{2.5}$. During P1, the mean concentration of SNA was 49.9 ± 31.6 μg/m^3. The mineral aerosols reached 16.4 ± 14.6 μg/m^3, accounting for 19% in $PM_{2.5}$. The contribution of OM to $PM_{2.5}$ was almost identical to that of mineral aerosols (Figure 4b).

https://doi.org/10.5194/egusphere-2023-127
Preprint. Discussion started: 10 March 2023

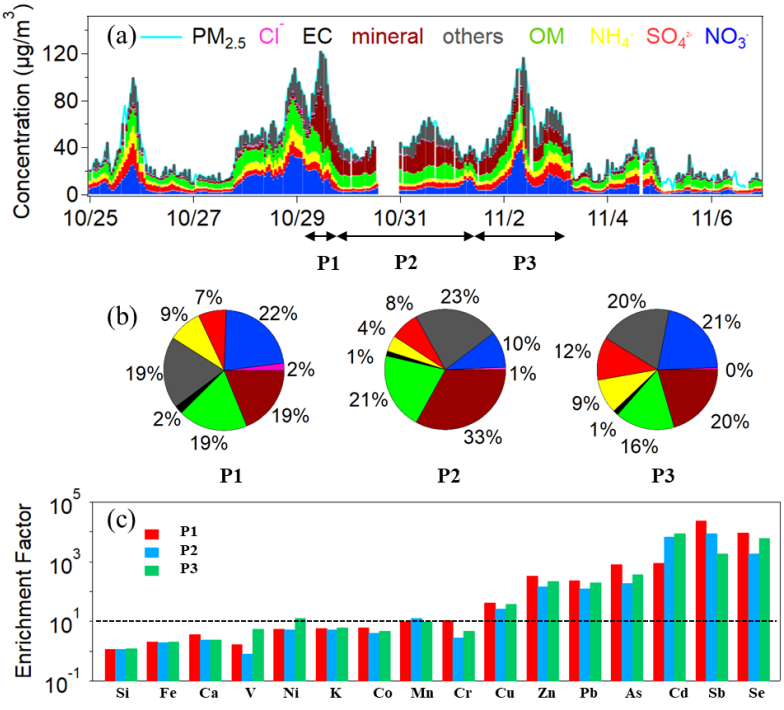

Figure 4. (a) Times-series of major chemical components in $PM_{2.5}$ during the study period. (b) The mean proportion of major chemical components in $PM_{2.5}$ during the three dust stages. (c) Enrichment factors of elements in $PM_{2.5}$ during the three dust stages.

During P2, mineral aerosols increased to 23.4±54.1μg/m^3 and accounted for 33% in $PM_{2.5}$, the highest among all three stages (Figure 4b). Due to the continuous dilution effect of dust on local anthropogenic pollutants, the concentrations and proportions of SNA in $PM_{2.5}$ were the lowest during this stage. For instance, NO_3^- only accounted for 10% in $PM_{2.5}$, indicating the formation of nitrate was suppressed to a certain extent. The level of OM didn't show obvious changes and averaged 10.1±2.1μg/m^3, accounting for 21% in $PM_{2.5}$.

During P3, mineral aerosols averaged 11.9±2.7μg/m^3, ranking the lowest among

https://doi.org/10.5194/egusphere-2023-127
Preprint. Discussion started: 10 March 2023

all three stages. The proportion of mineral aerosols in $PM_{2.5}$ decreased to 20%, suggesting the dust backflow from the ocean was less enriched in mineral components. Compared to P2, SNA showed significant increases and much stronger diurnal variations during P3. SO_4^{2-}, NO_3^-, and NH_4^+ averaged 6.7 ± 2.4, 12.4 ± 8.9, and 5.4 ± 2.7μg/m^3, respectively. As shown in Figure 4b, the contribution of nitrate to $PM_{2.5}$ increased to 21% while that of sulfate rose to 12%, the highest among all three stages. The concentration (9.3±3.2μg/m^3) and proportion (16%) of OM during P3 were lower than the other two stages, which was probably due to the unusual dust backflow transport pathway.

Enrichment factors (EFs) of the measured elements in $PM_{2.5}$ were calculated by using Al as a reference element, i.e., $EF_x=(X/Al)_{aerosol}/(X/Al)_{crust}$), where X was the element of interest. As shown in Figure 4c, elements such as Si, Fe, and Ca were less enriched as they mainly derived from the crust. While for anthropogenic elements including Cu, Zn, Pb, As, Cd, Sb, and Se, they were enriched by different extents with EFs between 10 and 10,000. In addition, these elements above were more enriched during P1 than P2 and P3. The dust transport pathway via inland areas during P1 should be the main cause as anthropogenic sources such as metallurgical industries, coal-fired plants, and smelters were widely located in inland regions. Exceptions were found for Ni and V, which were often used as tracers for heavy oil combustion. EFs of Ni and V exhibited higher values during P3 than P1 and P2. Since the dust backflow transport pathway during P3 had almost two-days travelling durations over the East China Sea, which was on the one of the busiest international shipping trade routes (Fan et al., 2016), the enrichments of Ni and Vi were probably ascribed to the mixing between dust and marine shipping emissions.

https://doi.org/10.5194/egusphere-2023-127
Preprint. Discussion started: 10 March 2023

3.3. Effect of unusually high O_3 on the formation of secondary aerosols during P2

Figure 5 shows the hourly near surface ozone concentrations and vertical profiles of ozone during the study period. Interestingly, a few high O_3 peaks occurred during the dust event (Figure 5a). O_3 averaged 92.8 ± 52.8μg/m^3 during the dust, about 50% higher than the non-dust days. Among the three dust stages, O_3 substantially increased from 35.9 ± 36.4μg/m^3 during P1 to 80.7 ± 41.2μg/m^3 during P2 and 104.0 ± 48.7μg/m^3 during P3. The low O_3 during P1 was due to the cleansing effect of strong dust associated with the strong cold front, which was as similar as previous studies that low oxidants concentrations were usually observed during strong dust events (Benas et al., 2013). As for the relatively high O_3 during P2 and P3, several causes may be responsible. Firstly, the mean wind speed was low of 0.4 and 0.6 m/s during P2 and P3, respectively. Thus, this weak synoptic system exerted weak dilution effect on the local air pollutants. Secondly, since the dust plume travelled mostly over the coastal and oceanic areas, part of O_3 could be transported from the high ozone oceanic areas (Wang et al., 2022b). Thirdly, the ozone lidar also observed high O_3 stripes during P2 and P3. As shown in Figure 5b, the high O_3 profiles extended from the surface to around 1km and the profile structure was similar to that of aerosol depolarization ratio. The subsidence of dust particles probably down drafted high-altitude O_3 and also contributed to the high O_3 near the ground.

https://doi.org/10.5194/egusphere-2023-127
Preprint. Discussion started: 10 March 2023

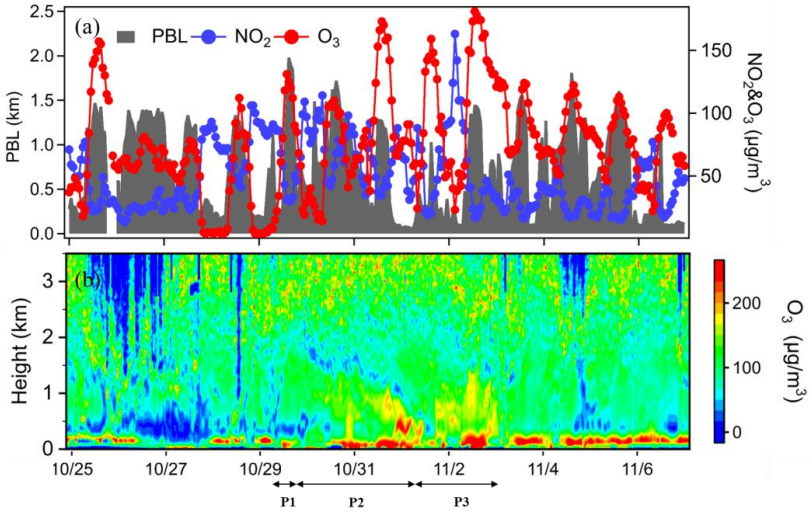

Figure 5. (a) Time-series of near surface O_3, NO_2 and planetary boundary layer height (b) Vertical profiles of ozone observed by the ozone Lidar.

To investigate the effect of the relatively high O_3 on the formation of secondary aerosols, Figure 6 displays the relationship between sulfate/nitrate and ammonium. The strong correlations of sulfate-ammonium (R^2 =0.91) and nitrate-ammonium (R^2 = 0.93) were expected. The scatters were further color coded by O_3 and it could be seen that higher sulfate, nitrate, and ammonium tended to be formed under higher O_3 concentrations, suggesting the potential role of photochemistry in promoting the formation of secondary aerosols.

https://doi.org/10.5194/egusphere-2023-127
Preprint. Discussion started: 10 March 2023

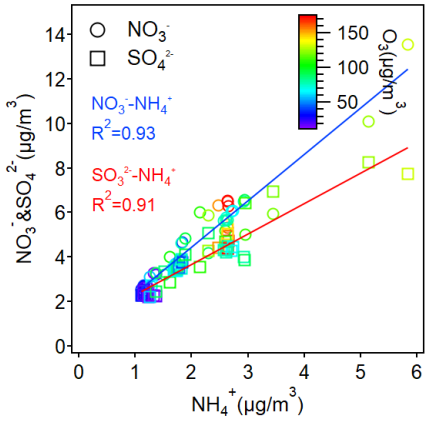

Figure 6. Linear relationship between sulfate/nitrate and ammonium with scatters colored by the concentrations of O_3 during P2

Figure 7 displays the linear relationship between sulfate and PM_{10}, ALWC, O_3, and HONO, respectively. Obviously, sulfate had no correlation with PM_{10} (Figure 7a), indicating that dust contributed negligibly to sulfate. Also, sulfate had almost no or even a weakly negative correlation with ALWC (Figure 7b), suggesting aqueous-phase processing was not a major reaction pathway of secondary aerosols during P2. In contrast, we found that sulfate correlated positively with O_3 (R^2=0.38, Figure 7c) and negatively correlated with HONO (R^2=0.25, Figure 7d). It was well recognized that HONO was an important precursor to OH radical and it was estimated that HONO accounted for 30%~60% of the OH budget in Shanghai (Bernard et al., 2016). The moderate correlations between sulfate and O_3/HONO corroborated the discussion above that the formation of secondary aerosols during P2 should be mainly promoted via the gas-phase oxidations.

https://doi.org/10.5194/egusphere-2023-127
Preprint. Discussion started: 10 March 2023

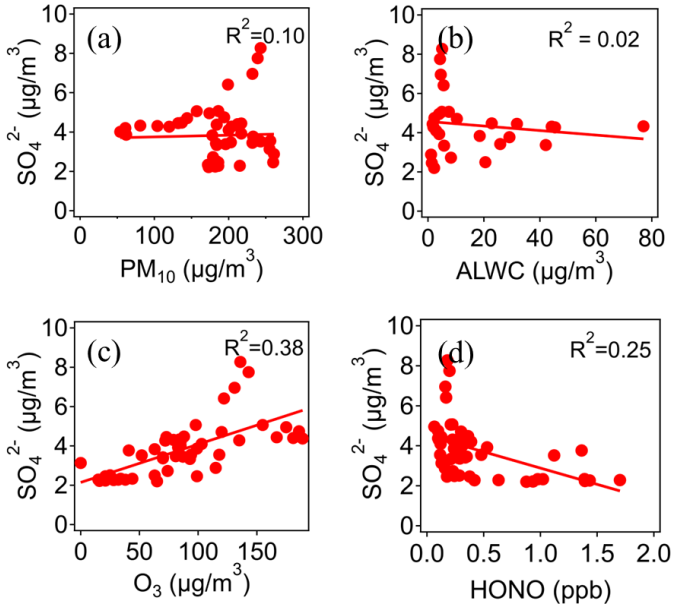

Figure 7. Linear relationship between sulfate and (a) PM_{10}, (b) ALWC, (c) O_3, and (d) HONO during P2

As similar as sulfate, nitrate didn't show correlation with ALWC (Figure 8b) but moderately correlated with O_3 (R^2=0.43, Figure 8c). Figure 8a displays the temporal variation of NO_2, O_3, HONO, and NO_3^- during P2. It can be found that although NO_2 was high at night as well as for HONO, the concentrations of NO_3^- were relatively low, indicating a low formation potential of secondary aerosols. Figure 2a shows that RH during P2 was relatively low at nighttime with a minimum of 31%, suggesting the aqueous reactions could be suppressed to some extents. During the daytime, O_3 reached its maximum while HONO reached its minimum, both contributing to the high levels of oxidants. The co-variation of nitrate and sulfate with O_3 (Figure 8a) confirmed that although dust often suppressed the formation of atmospheric oxidants, the photochemistry reactions under unusually high O_3 concentrations dominated the

https://doi.org/10.5194/egusphere-2023-127
Preprint. Discussion started: 10 March 2023

formation of sulfate and nitrate during P2 in this study.

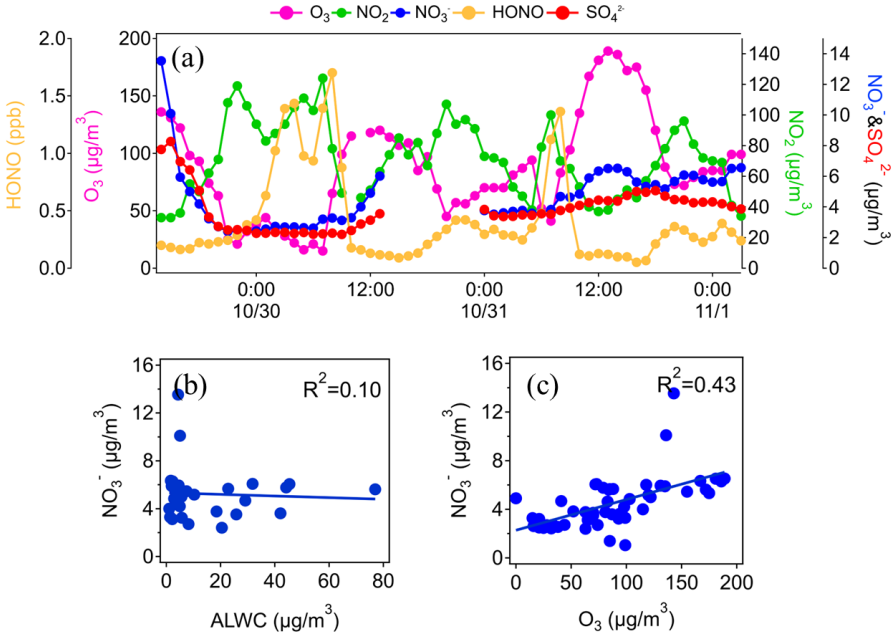

Figure 8. (a) Temporal variations of O_3, NO_2, HONO, nitrate, and sulfate during P2. Linear relationship between nitrate and (b) ALWC and (c) O_3.

3.4. Aerosol chemistry under dust backflows during P3

3.4.1. Evidence of dust backflows

The dust during P3 was diagnosed as a backflow transport pathway from mainland to Shanghai through the Yellow Sea and the East China Sea according to the backward trajectory analysis (Figure 3f). This atypical dust transport pathway observed in this study was defined as the dust backflow. In this section, we have provided more evidences of dust backflow from various aspects.

Figure 3f shows the dust drifted away from the Shandong Peninsula, thus we selected two coastal sites in Shandong province for supplementary analysis. Figure 9 compares the time-series of hourly air pollutants at Qingdao, Lianyungang, and

https://doi.org/10.5194/egusphere-2023-127
Preprint. Discussion started: 10 March 2023

Shanghai. At Qingdao and Lianyungang, high PM_{10} concentrations were observed during October 30 – 31, indicating the invasion of dust. After about two days, PM_{10} showed a peak at early November 2 at Shanghai. This was consistent with simulation duration of the backward trajectories, i.e., around 48 hours (Figure 3f). In Figure 9, it could be seen that in the dust upstream regions (i.e., Qingdao and Lianyungang), PM_{10} varied negatively with NO_2 and CO (the highlighted period in the figure). While in Shanghai, positive correlations between PM_{10} and NO_2 (R^2=0.32) as well as between PM_{10} and CO (R^2=0.55) indicated that the dust during P3 had acted as a carrier of the gaseous pollutants but not a diluter.

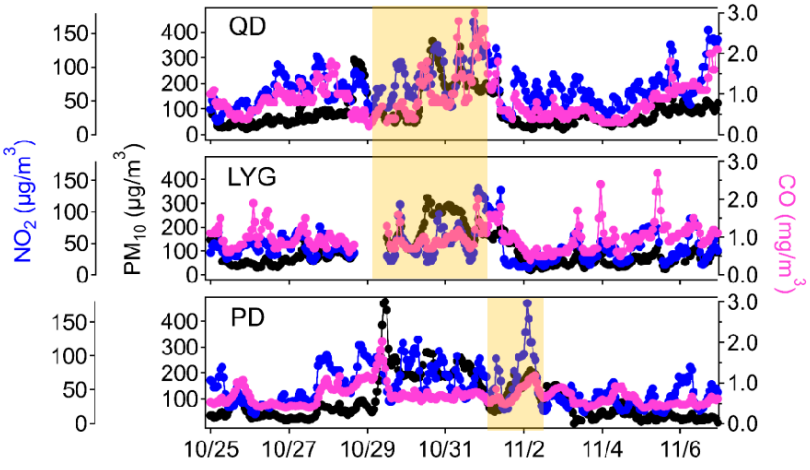

Figure 9. Time-series of PM_{10}, NO_2, and CO at Qingdao, Lianyungang, and Pudong. The dust periods at these three sites are highlighted.

More evidence of dust backflows was provided from the perspective of aerosol chemical tracers. As discussed in Section 3.2, enrichment factors of V and Ni were the highest during P3. Figure 10a further displays the time-series of V and Ni and they varied significantly during the study period. The mass concentrations of V and Ni

https://doi.org/10.5194/egusphere-2023-127
Preprint. Discussion started: 10 March 2023

increased 4 and 1.8 times during P3 compared to P2, respectively. This indicated that the dust had mixed with pollutants from marine vessel emissions and transported back to Shanghai.

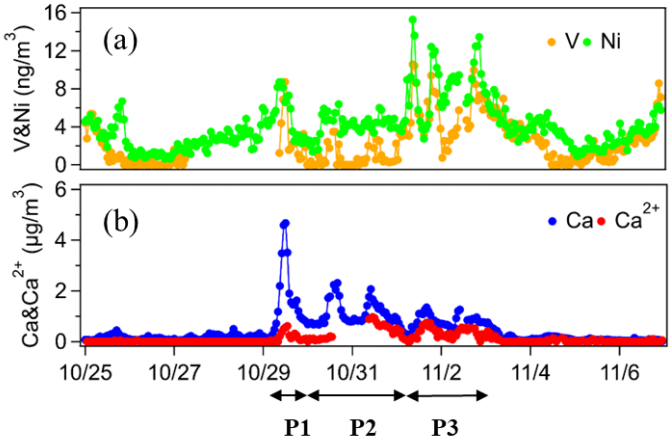

Figure 10. Time-series of (a) V, Ni, (b) Ca, and Ca^{2+} during the study period

Figure 10b plots the time-series of Ca and Ca^{2+}, which represented the total calcium and the soluble part of calcium, respectively. It was observed that Ca and Ca^{2+} didn't exhibit quite proportional variation trend, which should be related to the solubility of calcium during different dust stages. During P1, the mean concentration of Ca reached the highest of 1.63 ± 1.53μg/m^3 while Ca^{2+} was the lowest of 0.21 ± 0.20μg/m^3, thus resulting in the lowest Ca^{2+}/Ca ratio of 0.10 ± 0.08. As discussed in Section 3.1, dust during P1 was the strongest and thus it contained higher fractions of minerals, which were mainly in the form of insoluble metal oxides. The average concentrations of Ca^{2+} and Ca during P2 were 0.33 ± 0.28μg/m^3 and 1.11 ± 0.46μg/m^3 with the higher Ca^{2+}/Ca ratio of 0.27 ± 0.20. As a comparison, the average

https://doi.org/10.5194/egusphere-2023-127
Preprint. Discussion started: 10 March 2023

446 concentrations of $Ca^{2+}$and Ca during P3 reached 0.34 ± 0.20μg/m^3 and 0.78 ±
447 0.27μg/m^3, yielding the highest Ca^{2+}/Ca ratio of 0.38 ± 0.19. The much higher solubility
448 of calcium during P3 should be directly related to the lingerer of dust plumes over the
449 open ocean. The abundant water vapor over the ocean could accelerate the dissolution
450 of the insoluble components in particles during the mixing between continental dust
451 and oceanic air masses.

452

453 **3.4.2. Formation processes of secondary aerosols during P3**

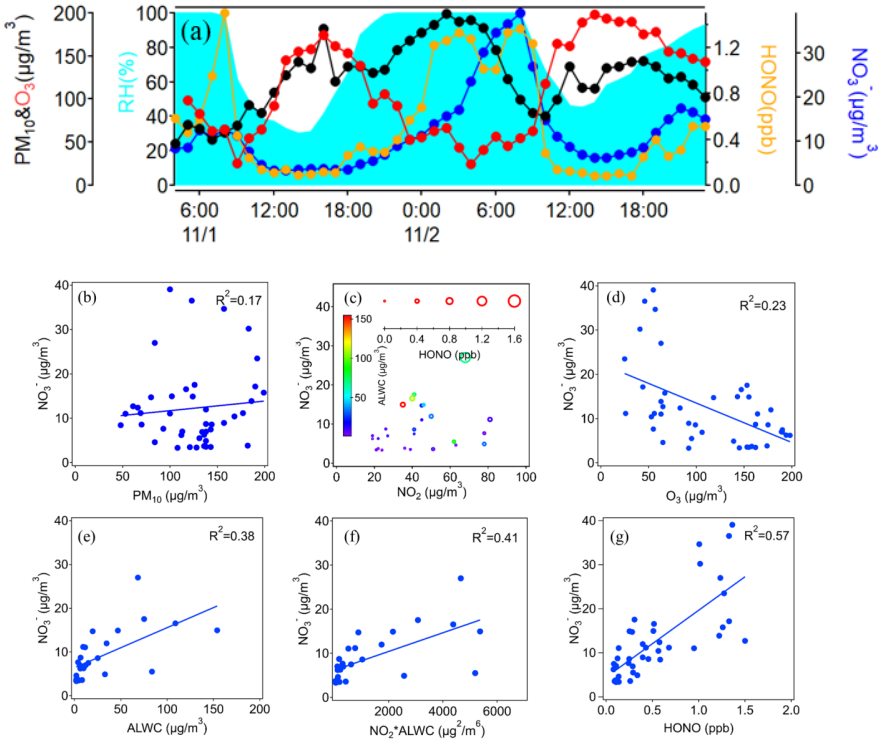

454

455

456 Figure 11. (a) Time series of PM_{10}, NO_3^-, O_3, HONO, and RH during P3. Linear
457 relationship between nitrate and (b) PM_{10}, (c) NO_2, (d) O_3, (e) ALWC, (f)
458 NO_2*AWLC, and (g) HONO.

459

https://doi.org/10.5194/egusphere-2023-127
Preprint. Discussion started: 10 March 2023

In this section, the main processes that dominated the formation of secondary aerosols during P3 were probed and compared to P2. Figure 11a shows the time-series of hourly PM_{10}, NO_3^-, O_3, HONO, and RH during P3. It could be visualized that most parameters co-varied relatively consistently to some extent. Different from P2, nitrate showed weak correlation with PM_{10} (Figure b), indicating that part of nitrate could be directly transported via the dust transport. Also different from P2, nitrate even showed negative correlation with O_3 (Figure d). From Figure 11a, nitrate concentrations were at its troughs during daytime when O_3 peaked. Thus, photochemical reactions didn't play an important role in the formation of nitrate during this stage.

Figure c investigates the conjoint impact of multiple parameters on the formation of nitrate. In general, NO_3^- was more favored under higher NO_2, which was obviously expected as NO_3^- could be either formed by the photochemical oxidation of NO_2 by OH radicals at daytime (Hertel et al., 2012) or produced by hydrolysis of N_2O_5 from the oxidation of NO_2 by O_3 at nighttime (Ge et al., 2017). In addition, the formation of higher NO_3^- was accompanied with higher ALWC and HONO, implying the role of aqueous phase reactions rather than the photochemical reactions. Figure e-11g separately investigate the relationship between NO_3^- and various parameters. NO_3^- moderately correlated with ALWC ($R^2 = 0.38$). By relating NO_3^- and the multiplication of ALWC and NO_2, the correlation coefficient ($R^2 = 0.41$) was further improved (Figure f), indicating the reaction pathway of NO_2 to nitrate in the aqueous phase. Figure 11g also observed strong correlation between NO_3^- and HONO ($R^2 = 0.57$). Alicke et al. (2002) proposed that the heterogeneous reactions of NO_2 on the surface of moist particles produced both nitrate and HONO, i.e.,

$$2NO_2+H_2O \rightarrow HONO+HNO_3$$

https://doi.org/10.5194/egusphere-2023-127
Preprint. Discussion started: 10 March 2023

Compared to the mean ALWC (11.8 ± 17.1μg/m^3) during P2, ALWC during P3 was much higher of 29.1 ± 38.0μg/m^3. This was mainly ascribed to the higher atmospheric water vapor during P3, which was evidently caused by the backflows of oceanic air masses. The different levels of ALWC between P2 and P3 caused divergent role of aqueous processing in the secondary aerosol formation.

As for sulfate, its temporal variation during P3 was quite different from NO_3^- that it showed no diurnal pattern while presented a gradually increasing trend (Figure a). This suggested sulfate had gone through a different formation mechanism from nitrate. SO_4^{2-} correlated strongly with Na^+ (Figure c), which can be regarded as the tracer of sea salts. The co-variation of SO_4^{2-} and Na^+ probably suggested that a portion of sulfate was aged and directly transported by the oceanic air masses. Additionally, SO_4^{2-} had weakly positive correlation with O_3 (Figure d) and ALWC (Figure e), indicating that both gas and aqueous phase processes contributed to the secondary formation of sulfate to some extent. Figure 12a also adds the time-series of Ca^{2+}/Ca, which didn't co-vary with either sulfate or nitrate. This probably indicated that the chemical reactions between acidic gaseous precursors and dust mineral components were negligible.

https://doi.org/10.5194/egusphere-2023-127
Preprint. Discussion started: 10 March 2023

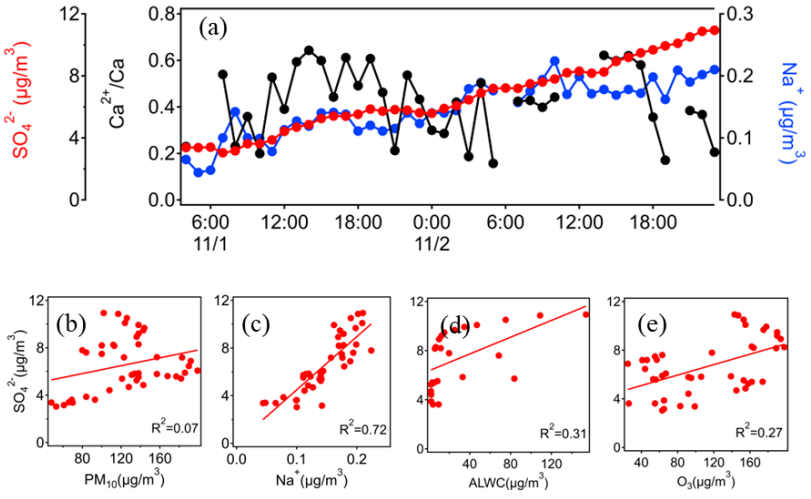

Figure 12. (a) Time-series of sulfate, Na^+, and Ca^{2+}/Ca during P3. Linear between sulfate and (b) PM_{10}, (c) Na^+, (d) O_3, and (e) ALWC.

To assess whether dust or sea salts participated in the heterogeneous reactions of secondary aerosol during P3, the ISORROPIA II model was run with different scenarios. Figure S1 shows the model performance for SO_4^{2-}, NO_3^-, NH_4^+, and NH_3 based on the SO_4^{2-}–NO_3^-–NH_4^+–Cl^-–NH_3–HCl–HNO_3 system. After adding Ca^{2+} into this thermodynamic equilibrium system, the correlations between the simulations vs observations for all four species were lowered with different extents (Figure S2). This indicated that Ca^{2+} was not internally mixed with sulfate and nitrate and probably suggested that the heterogeneous reactions on dust were very limited.

Then Na^+ was added into the thermodynamic equilibrium system (Figure S3). It could be seen the model performance was slightly improved. The correlation coefficients of the four species were closer to the unity and the regression slopes were also more parallel to the y=x line. This suggested that sea salts were involved in the formation of secondary inorganic aerosols during the dust backflow. This also explained

https://doi.org/10.5194/egusphere-2023-127
Preprint. Discussion started: 10 March 2023

the strong correlation between SO_4^{2-} and Na^+ during P3.

3.4.3. Estimation of transported and secondarily formed particles during P3

As discussed in the previous sections, the sources of aerosols during P3 could be derived from both aged aerosols via the dust backflows and secondary formation. In this section, we aimed to estimate the contribution of transport and secondary formation to the main aerosol species, respectively, based on the simultaneous measurements at the Pudong site and the Lianyungang site. As discussed in Section 3.4.1, Lianyungang acted as an upstream region of dust transport drifting from the mainland. The dust duration observed at Lianyungang was from about 5:00, October 30 to 16:00, October 31, about 46 hours ahead of the dust invasion observed at Pudong (Figure 9).

To assess the extents of transported pollutants, black carbon (BC) was used as a reference aerosol component. As shown in Figure S4, one BC pollution episode on October 30 at Lianyungang was observed. Consistently, another BC pollution episode on November 2 at Pudong emerged after about 46 hours. Since the air mass trajectory from Lianyungang to Pudong was mostly over the ocean and BC had no secondary sources, it could be reasonably assumed that the difference of BC between these two sites was ascribed to the removal processes of particles.

We further defined the average concentrations of various aerosol components during the previous five hours of the dust at Pudong as their background concentrations. Then, a coefficient *k* was derived to calculate the removal fractions of aerosols during the dust transport as below.

$$k = \frac{AV_{LYG,BC} - (AV_{PD,BC} - BKG_{PD,BC})}{AV_{LYG,BC}}$$

https://doi.org/10.5194/egusphere-2023-127
Preprint. Discussion started: 10 March 2023

$AV_{LYG,BC}$ and $AV_{PD,BC}$ represent the average concentration of BC at Lianyungang and Pudong during their respective dust period. $BKG_{PD,BC}$ represents the background concentration of BC at Pudong. By assuming that other aerosol species were removed at a similar efficiency as BC, the amounts of transported aerosol species from Lianyungang to Pudong can be estimated as below.

$$TP_{PD,i} = AV_{LYG,i} \times (1- k)$$

$TP_{PD,i}$ represents the transported amounts for aerosol species *i*. Then, the secondarily formed aerosol species *i* at Pudong can be calculated as below.

$$SF_{PD,i} = AV_{PD,i} - BKG_{PD,i} - TP_{PD,i}$$

Figure 13 shows the results of the transported and the secondarily formed aerosol species during P3. It was calculated that the secondarily formed and transported NO_3^- averaged 6.8μg/m^3 and 4.7μg/m^3, accounting for about 45% and 31% of its total mass concentration, respectively. This was consistent with the analysis above that a considerable portion of nitrate was formed through the aqueous phase secondary formation. In contrast, it was calculated that the transported SO_4^{2-} accounted for about 42% of its total mass concentration while the secondarily formed SO_4^{2-} was almost negligible. This was also consistent with the phenomenon that SO_4^{2-} correlated significantly with Na^+ (Figure 12c), suggesting most sulfate was aged and transported. As for NH_4^+, its origin apportionment was similar to NO_3^- that the secondarily formed and transported NH_4^+ accounted for about 35% and 28% of its total mass concentration, respectively. Compared to NO_3^- and NH_4^+, OM was more dominated by transport (57%) while its secondary formation only accounted for about 13%.

https://doi.org/10.5194/egusphere-2023-127
Preprint. Discussion started: 10 March 2023

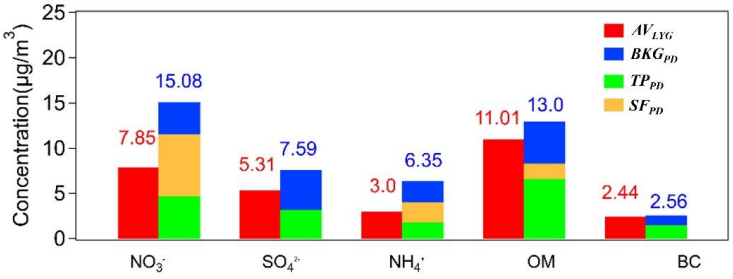

Figure 13. The apportioned concentrations of the major aerosol species during P3.

4. Conclusion

During October 29 to November 2, 2019, a long-lasting dust event was observed in Shanghai based on a synergy measurement of near surface air pollutants, aerosol lidar, wind profiling lidar, and air masses trajectory modeling. During the whole dust period, the mean concentrations of $PM_{2.5}$ and PM_{10} reached 53.3 ± 20.5μg/m^3 and 172.4 ± 70.2μg/m^3. Different from most dust events, this dust event was characterized of exceptionally high relative humidity (71 ± 26%) and low wind speed (0.54 ± 0.59m/s). Due to this stagnant synoptic condition, the mean concentrations of main gaseous pollutants such as O_3, SO_2, and NO_2 reached 86.0 ± 47.8μg/m^3, 11.8 ± 3.4μg/m^3, and 63.3 ± 27.9μg/m^3, respectively, even higher than those during the non-dust period.

The dust event was divided into three stages from P1 – P3. P1 was a short dust episode from 4:00 - 13:00, October 29, when wind profiles showed dominant northwest winds from the ground to the altitudes of around 2km, indicating the presence of a strong synoptic system. P2 was a dust episode from 14:00, October 29 to 3:00, November 1, when RH was moderately high of 70 ± 26% and the southeasterlies

https://doi.org/10.5194/egusphere-2023-127
Preprint. Discussion started: 10 March 2023

prevailed with partial air masses from coastal regions. P3 was a rarely observed dust backflow transport episode from 4:00, November 1 to 23:00, November 2. The air masses originated from the Shandong Peninsula and the northern region of Jiangsu province, and then migrated over the Yellow Sea and the East China Sea. RH reached the highest of 76 ± 24% among the three stages of the dust event.

During P2, mineral aerosols accounted for 33% in $PM_{2.5}$, the highest among all three stages. Abnormally high O_3 concentrations were observed, much higher than the non-dust days. This was partially due to the weak synoptic system that exerted weak dilution effect on the local air pollutants. Also, part of O_3 could be transported from the high ozone oceanic areas. The ozone lidar observed that the subsidence of dust particles probably down drafted high-altitude O_3 and also contributed to the high O_3 near the ground. As a result, sulfate and nitrate moderately correlated with O_3 while had almost no correlation with ALWC, indicating that the formation of secondary aerosols during P2 should be mainly promoted via the gas-phase oxidations.

During P3, a special phenomenon of dust backflow was observed and confirmed by various evidences. Two upstream sites (Qingdao and Lianyungang) showed dust occurrences about 48 hours ahead that of Shanghai, consistent with the transport duration of the dust backflow from the Shandong Peninsula to Shanghai over the Yellow Sea and the East China Sea. In addition, the mass concentrations of V and Ni significantly increased, indicating the mixing between dust and marine vessel emissions. The highest Ca^{2+}/Ca ratio of 0.38 ± 0.19 was observed during P3, which should be due to that the lingerer of dust plumes over the open ocean facilitated efficient solubility of calcium. Different from P2, nitrate didn't correlate with O_3, while it was favored under high NO_2 and ALWC and strongly correlated with HONO, indicating the reaction

https://doi.org/10.5194/egusphere-2023-127
Preprint. Discussion started: 10 March 2023

609 pathway of NO_2 to nitrate in the aqueous phase. As for sulfate, the strong correlation
610 between SO_4^{2-} and Na^+ suggested that a portion of sulfate was aged and directly
611 transported by the oceanic air masses. The ISORROPIA II modeling added Na^+ into the
612 SO_4^{2-}–NO_3^-–NH_4^+–Cl^-–NH_3–HCl–HNO_3 system and found the models performances
613 of simulating the major aerosol and gaseous species could be improved. As a
614 comparison, the models performances became worse after adding Ca^{2+}. This suggested
615 that sea salts participated in the secondary aerosol formation while dust heterogeneous
616 reactions were limited during P3. Based on a simple method, the amounts of transported
617 and secondarily formed particles during P3 were quantified. It was calculated that about
618 45% and 31% of NO_3^- was contributed by secondary formation and transport,
619 respectively. In contrast, the transported SO_4^{2-} accounted for about 42% of its total mass
620 concentration while the rest was from its background concentration with negligible
621 secondary formation. OM was dominated by transport (57%) while its secondary
622 formation only accounted for about 13%.
623
624 **Data Availability Statement**
625 All data used in this study can be requested upon the corresponding author
626 (huangkan@fudan.edu.cn).
627
628 **Author contributions**
629 KH, QF, and YD designed this study. JH, FY, YL, and JC performed data
630 collection. DL and KH performed data analysis and wrote the paper. All have
631 commented on and reviewed the paper.
632

https://doi.org/10.5194/egusphere-2023-127
Preprint. Discussion started: 10 March 2023

Competing interests

The authors declare that they have no conflict of interest.

Acknowledgments

This work was financially supported by the National Science Foundation of China (42175119).

References

Alicke, B., Platt, U., and Stutz, J.: Impact of nitrous acid photolysis on the total hydroxyl radical budget during the Limitation of Oxidant Production/Pianura Padana Produzione di Ozono study in Milan, J. Geophys. Res.-Atmos., 107, 18, 10.1029/2000jd000075, 2002.

Ansari, A. S. and Pandis, S. N.: An analysis of four models predicting the partitioning of semivolatile inorganic aerosol components, Aerosol Science And Technology, 31, 129-153, 10.1080/027868299304200, 1999.

Arimoto, R., Ray, B. J., Lewis, N. F., Tomza, U., and Duce, R. A.: Mass-particle size distributions of atmospheric dust and the dry deposition of dust to the remote ocean, J. Geophys. Res.-Atmos., 102, 15867-15874, 10.1029/97jd00796, 1997.

Barkley, A., Olson, N., Prospero, J., Gatineau, A., Panechou, K., Maynard, N., Blackwelder, P., China, S., Ault, A., and Gaston, C.: Atmospheric Transport of North African Dust - Bearing Supermicron Freshwater Diatoms to South America: Implications for Iron Transport to the Equatorial North Atlantic Ocean, Geophysical Research Letters, 48, 10.1029/2020GL090476, 2021.

Benas, N., Mourtzanou, E., Kouvarakis, G., Bais, A., Mihalopoulos, N., and Vardavas, I.: Surface ozone photolysis rate trends in the Eastern Mediterranean: Modeling the effects of aerosols and total column ozone based on Terra MODIS data, Atmospheric Environment, 74, 1-9, 10.1016/j.atmosenv.2013.03.019, 2013.

Bernard, F., Cazaunau, M., Grosselin, B., Zhou, B., Zheng, J., Liang, P., Zhang, Y., Ye, X., Daële, V., Mu, Y., Zhang, R., Chen, J., and Mellouki, A.: Measurements of nitrous acid (HONO) in urban area of Shanghai, China, Environmental Science and Pollution Research, 23, 5818-5829, 10.1007/s11356-015-5797-4, 2016.

Dall'Osto, M., Harrison, R. M., Coe, H., and Williams, P.: Real-time secondary aerosol formation during a fog event in London, Atmospheric Chemistry And Physics, 9, 2459-2469,

https://doi.org/10.5194/egusphere-2023-127
Preprint. Discussion started: 10 March 2023

10.5194/acp-9-2459-2009, 2009.

Fan, Q. Z., Zhang, Y., Ma, W. C., Ma, H. X., Feng, J. L., Yu, Q., Yang, X., Ng, S. K. W., Fu, Q. Y., and Chen, L. M.: Spatial and Seasonal Dynamics of Ship Emissions over the Yangtze River Delta and East China Sea and Their Potential Environmental Influence, Environmental Science & Technology, 50, 1322-1329, 10.1021/acs.est.5b03965, 2016.

Feng, X., Mao, R., Gong, D.-Y., Zhao, C., Wu, C., Zhao, C., Wu, G., Lin, Z., Liu, X., Wang, K., and Sun, Y.: Increased Dust Aerosols in the High Troposphere Over the Tibetan Plateau From 1990s to 2000s, Journal of Geophysical Research: Atmospheres, 125, e2020JD032807, https://doi.org/10.1029/2020JD032807, 2020.

Fu, Q., Zhuang, G., Li, J., Huang, K., Wang, Q., Zhang, R., Fu, J., Lu, T., Chen, M., Wang, Q., Chen, Y., Xu, C., and Hou, B.: Source, long-range transport, and characteristics of a heavy dust pollution event in Shanghai, Journal of Geophysical Research: Atmospheres, 115, https://doi.org/10.1029/2009JD013208, 2010.

Ge, X. L., He, Y. A., Sun, Y. L., Xu, J. Z., Wang, J. F., Shen, Y. F., and Chen, M. D.: Characteristics and Formation Mechanisms of Fine Particulate Nitrate in Typical Urban Areas in China, Atmosphere, 8, 12, 10.3390/atmos8030062, 2017.

Ginoux, P., Prospero, J. M., Torres, O., and Chin, M.: Long-term simulation of global dust distribution with the GOCART model: correlation with North Atlantic Oscillation, Environmental Modelling & Software, 19, 113-128, https://doi.org/10.1016/S1364-8152(03)00114-2, 2004.

Goodman, M. M., Carling, G. T., Fernandez, D. P., Rey, K. A., Hale, C. A., Bickmore, B. R., Nelson, S. T., and Munroe, J. S.: Trace element chemistry of atmospheric deposition along the Wasatch Front (Utah, USA) reflects regional playa dust and local urban aerosols, Chemical Geology, 530, 10.1016/j.chemgeo.2019.119317, 2019.

Hertel, O., Skjoth, C. A., Reis, S., Bleeker, A., Harrison, R. M., Cape, J. N., Fowler, D., Skiba, U., Simpson, D., Jickells, T., Kulmala, M., Gyldenkaerne, S., Sorensen, L. L., Erisman, J. W., and Sutton, M. A.: Governing processes for reactive nitrogen compounds in the European atmosphere, Biogeosciences, 9, 4921-4954, 10.5194/bg-9-4921-2012, 2012.

Hilario, M. R. A., Cruz, M. T., Cambaliza, M. O. L., Reid, J. S., Xian, P., Simpas, J. B., Lagrosas, N. D., Uy, S. N. Y., Cliff, S., and Zhao, Y. J.: Investigating size-segregated sources of elemental composition of particulate matter in the South China Sea during the 2011 Vasco cruise, Atmospheric Chemistry And Physics, 20, 1255-1276, 10.5194/acp-20-1255-2020, 2020.

Hsu, S.-C., Lee, C. S. L., Huh, C.-A., Shaheen, R., Lin, F.-J., Liu, S. C., Liang, M.-C., and Tao, J.: Ammonium deficiency caused by heterogeneous reactions during a super Asian dust episode, Journal of Geophysical Research: Atmospheres, 119, 6803-6817, 10.1002/2013jd021096, 2014.

https://doi.org/10.5194/egusphere-2023-127
Preprint. Discussion started: 10 March 2023

Huang, K., Fu, J. S., Lin, N.-H., Wang, S.-H., Dong, X., and Wang, G.: Superposition of Gobi Dust and Southeast Asian Biomass Burning: The Effect of Multisource Long-Range Transport on Aerosol Optical Properties and Regional Meteorology Modification, Journal of Geophysical Research: Atmospheres, 124, 9464-9483, https://doi.org/10.1029/2018JD030241, 2019.

Huang, K., Zhuang, G., Li, J., Wang, Q., Sun, Y., Lin, Y., and Fu, J. S.: Mixing of Asian dust with pollution aerosol and the transformation of aerosol components during the dust storm over China in spring 2007, Journal of Geophysical Research, 115, 10.1029/2009jd013145, 2010.

Liang, Y., Liu, Y., Wang, H., Li, L., Duan, Y., and Lu, K.: Regional characteristics of ground-level ozone in Shanghai based on PCA analysis, Acta Scientiae Circumstantiae, 38, 3807-3815, 2018.

Liu, J., Ding, J., Rexiding, M., Li, X., Zhang, J., Ran, S., Bao, Q., and Ge, X.: Characteristics of dust aerosols and identification of dust sources in Xinjiang, China, Atmospheric Environment, 262, 118651, https://doi.org/10.1016/j.atmosenv.2021.118651, 2021.

Malm, W. C., Sisler, J. F., Huffman, D., Eldred, R. A., and Cahill, T. A.: Spatial and seasonal trends in particle concentration and optical extinction in the United States, Journal of Geophysical Research: Atmospheres, 99, 1347-1370, https://doi.org/10.1029/93JD02916, 1994.

Mentel, T. F., Bleilebens, D., and Wahner, A.: A study of nighttime nitrogen oxide oxidation in a large reaction chamber—the fate of NO2, N2O5, HNO3, and O3 at different humidities, Atmospheric Environment, 30, 4007-4020, https://doi.org/10.1016/1352-2310(96)00117-3, 1996.

Nagashima, K., Suzuki, Y., Irino, T., Nakagawa, T., Tada, R., Hara, Y., Yamada, K., and Kurosaki, Y.: Asian dust transport during the last century recorded in Lake Suigetsu sediments, Geophysical Research Letters, 43, 2835-2842, https://doi.org/10.1002/2015GL067589, 2016.

Nenes, A., Pandis, S. N., and Pilinis, C.: ISORROPIA: A new thermodynamic equilibrium model for multiphase multicomponent inorganic aerosols, Aquat. Geochem., 4, 123-152, 10.1023/a:1009604003981, 1998.

Patel, A. and Rastogi, N.: Chemical Composition and Oxidative Potential of Atmospheric PM10 over the Arabian Sea, ACS Earth Space Chem., 4, 112-121, 10.1021/acsearthspacechem.9b00285, 2020.

Perez, N., Pey, J., Reche, C., Cortes, J., Alastuey, A., and Querol, X.: Impact of harbour emissions on ambient PM10 and PM2.5 in Barcelona (Spain): Evidences of secondary aerosol formation within the urban area, Science Of the Total Environment, 571, 237-250, 10.1016/j.scitotenv.2016.07.025, 2016.

Petetin, H., Sciare, J., Bressi, M., Gros, V., Rosso, A., Sanchez, O., Sarda-Estève, R., Petit,

https://doi.org/10.5194/egusphere-2023-127
Preprint. Discussion started: 10 March 2023

J. E., and Beekmann, M.: Assessing the ammonium nitrate formation regime in the Paris megacity and its representation in the CHIMERE model, Atmos. Chem. Phys., 16, 10419-10440, 10.5194/acp-16-10419-2016, 2016.

Shen, L., Zhao, C., Ma, Z., Li, Z., Li, J., and Wang, K.: Observed decrease of summer sea-land breeze in Shanghai from 1994 to 2014 and its association with urbanization, Atmospheric Research, 227, 198-209, https://doi.org/10.1016/j.atmosres.2019.05.007, 2019.

Song, S., Gao, M., Xu, W., Shao, J., Shi, G., Wang, S., Wang, Y., Sun, Y., and McElroy, M. B.: Fine-particle pH for Beijing winter haze as inferred from different thermodynamic equilibrium models, Atmos. Chem. Phys., 18, 7423-7438, 10.5194/acp-18-7423-2018, 2018.

Su, L., Yuan, Z., Fung, J. C. H., and Lau, A. K. H.: A comparison of HYSPLIT backward trajectories generated from two GDAS datasets, Science of The Total Environment, 506-507, 527-537, https://doi.org/10.1016/j.scitotenv.2014.11.072, 2015.

Sun, P., Nie, W., Wang, T., Chi, X., Huang, X., Xu, Z., Zhu, C., Wang, L., Qi, X., Zhang, Q., and Ding, A.: Impact of air transport and secondary formation on haze pollution in the Yangtze River Delta: In situ online observations in Shanghai and Nanjing, Atmospheric Environment, 225, 117350, https://doi.org/10.1016/j.atmosenv.2020.117350, 2020.

Tang, M., Cziczo, D. J., and Grassian, V. H.: Interactions of Water with Mineral Dust Aerosol: Water Adsorption, Hygroscopicity, Cloud Condensation, and Ice Nucleation, Chemical Reviews, 116, 4205-4259, 10.1021/acs.chemrev.5b00529, 2016.

Tian, R., Ma, X., Sha, T., Pan, X., and Wang, Z.: Exploring dust heterogeneous chemistry over China: Insights from field observation and GEOS-Chem simulation, Science of The Total Environment, 798, 149307, https://doi.org/10.1016/j.scitotenv.2021.149307, 2021.

Vicars, W. C. and Sickman, J. O.: Mineral dust transport to the Sierra Nevada, California: Loading rates and potential source areas, Journal of Geophysical Research, 116, 10.1029/2010jg001394, 2011.

Wang, G., Chen, J., Xu, J., Yun, L., Zhang, M., Li, H., Qin, X., Deng, C., Zheng, H., Gui, H., Liu, J., and Huang, K.: Atmospheric processing at the sea-land interface over the South China Sea: secondary aerosol formation, aerosol acidity, and role of sea salts, Journal of Geophysical Research: Atmospheres, n/a, e2021JD036255, https://doi.org/10.1029/2021JD036255,

Wang, G. C., Chen, J., Xu, J., Yun, L., Zhang, M. D., Li, H., Qin, X. F., Deng, C. R., Zheng, H. T., Gui, H. Q., Liu, J. G., and Huang, K.: Atmospheric Processing at the Sea-Land Interface Over the South China Sea: Secondary Aerosol Formation, Aerosol Acidity, and Role of Sea Salts, J. Geophys. Res.-Atmos., 127, 10.1029/2021jd036255, 2022a.

Wang, G. H., Cheng, C. L., Huang, Y., Tao, J., Ren, Y. Q., Wu, F., Meng, J. J., Li, J. J., Cheng, Y. T., Cao, J. J., Liu, S. X., Zhang, T., Zhang, R., and Chen, Y. B.: Evolution of aerosol

https://doi.org/10.5194/egusphere-2023-127
Preprint. Discussion started: 10 March 2023

chemistry in Xi'an, inland China, during the dust storm period of 2013-Part 1: Sources, chemical forms and formation mechanisms of nitrate and sulfate, Atmospheric Chemistry And Physics, 14, 11571-11585, 10.5194/acp-14-11571-2014, 2014.

Wang, J. J., Zhang, M. G., Bai, X. L., Tan, H. J., Li, S., Liu, J. P., Zhang, R., Wolters, M. A., Qin, X. Y., Zhang, M. M., Lin, H. M., Li, Y. N., Li, J., and Chen, L. Q.: Large-scale transport of PM2.5 in the lower troposphere during winter cold surges in China, Sci Rep, 7, 10, 10.1038/s41598-017-13217-2, 2017.

Wang, L., Du, H., Chen, J., Zhang, M., Huang, X., Tan, H., Kong, L., and Geng, F.: Consecutive transport of anthropogenic air masses and dust storm plume: Two case events at Shanghai, China, Atmospheric Research, 127, 22-33, https://doi.org/10.1016/j.atmosres.2013.02.011, 2013.

Wang, N., Zheng, P., Wang, R., Wei, B., An, Z., Li, M., Xie, J., Wang, Z., Wang, H., and He, M.: Homogeneous and heterogeneous atmospheric ozonolysis of acrylonitrile on the mineral dust aerosols surface, Journal of Environmental Chemical Engineering, 9, 106654, https://doi.org/10.1016/j.jece.2021.106654, 2021.

Wang, Q., Wang, X., Huang, R., Wu, J., Xiao, Y., Hu, M., Fu, Q., Duan, Y., and Chen, J.-M.: Regional Transport of PM 2.5 and O 3 Based on Complex Network Method and Chemical Transport Model in the Yangtze River Delta, China, Journal of Geophysical Research: Atmospheres, 127, 10.1029/2021JD034807, 2022b.

Wang, Q., Dong, X., Fu, J. S., Xu, J., Deng, C., Jiang, Y., Fu, Q., Lin, Y., Huang, K., and Zhuang, G.: Environmentally dependent dust chemistry of a super Asian dust storm in March 2010: observation and simulation, Atmos. Chem. Phys., 18, 3505-3521, 10.5194/acp-18-3505-2018, 2018a.

Wang, Z., Pan, X. L., Uno, I., Chen, X. S., Yamamoto, S., Zheng, H. T., Li, J., and Wang, Z. F.: Importance of mineral dust and anthropogenic pollutants mixing during a long-lasting high PM event over East Asia, Environ. Pollut., 234, 368-378, 10.1016/j.envpol.2017.11.068, 2018b.

West, J. J., Ansari, A. S., and Pandis, S. N.: Marginal PM25: Nonlinear Aerosol Mass Response to Sulfate Reductions in the Eastern United States, Journal of the Air & Waste Management Association, 49, 1415-1424, 10.1080/10473289.1999.10463973, 1999.

Wu, C., Zhang, S., Wang, G., Lv, S., Li, D., Liu, L., Li, J., Liu, S., Du, W., Meng, J., Qiao, L., Zhou, M., Huang, C., and Wang, H.: Efficient Heterogeneous Formation of Ammonium Nitrate on the Saline Mineral Particle Surface in the Atmosphere of East Asia during Dust Storm Periods, Environmental Science & Technology, 54, 15622-15630, 10.1021/acs.est.0c04544, 2020.

Xu, B., Wang, L., Gu, Z., Hao, Q., Wang, H., Chu, G., Jiang, D., Liu, Q., and Qin, X.:

https://doi.org/10.5194/egusphere-2023-127
Preprint. Discussion started: 10 March 2023

Decoupling of Climatic Drying and Asian Dust Export During the Holocene, Journal of Geophysical Research: Atmospheres, 123, 915-928, https://doi.org/10.1002/2017JD027483, 2018.

Xu, J., Chen, J., Zhao, N., Wang, G. C., Yu, G. Y., Li, H., Huo, J. T., Lin, Y. F., Fu, Q. Y., Guo, H. Y., Deng, C. R., Lee, S. H., Chen, J. M., and Huang, K.: Importance of gas-particle partitioning of ammonia in haze formation in the rural agricultural environment, Atmospheric Chemistry and Physics, 20, 7259-7269, 10.5194/acp-20-7259-2020, 2020.

Yu, S. C., Dennis, R., Roselle, S., Nenes, A., Walker, J., Eder, B., Schere, K., Swall, J., and Robarge, W.: An assessment of the ability of three-dimensional air quality models with current thermodynamic equilibrium models to predict aerosol NO3, J. Geophys. Res.-Atmos., 110, 10.1029/2004jd004718, 2005.

Zhang, D., Iwasaka, Y., Shi, G., Zang, J., Hu, M., and Li, C.: Separated status of the natural dust plume and polluted air masses in an Asian dust storm event at coastal areas of China, Journal of Geophysical Research (Atmospheres), 110, D06302, 10.1029/2004jd005305, 2005.

Zhao, D., Xin, J., Wang, W., Jia, D., Wang, Z., Xiao, H., Liu, C., Zhou, J., Tong, L., Ma, Y., Wen, T.-X., Wu, F.-K., and Wang, L.: Effects of the sea-land breeze on coastal ozone pollution in the Yangtze River Delta, Science of The Total Environment, 807, 10.1016/j.scitotenv.2021.150306, 2021.

Zheng, Y., Zhao, T., Che, H., Liu, Y., Han, Y., Liu, C., Xiong, J., Liu, J., and Zhou, Y.: A 20-year simulated climatology of global dust aerosol deposition, Science of The Total Environment, 557-558, 861-868, https://doi.org/10.1016/j.scitotenv.2016.03.086, 2016.